Late Holocene air temperature variability reconstructed from the sediments of Laguna Escondida, Patagonia, Chile (45°30'S)

Julie Elbert[1], Richard Wartenburger[1], Lucien von Gunten[1,2], Roberto Urrutia[3], Daniela Fischer[1], Marian Fujak[4], Yvonne Hamann[5], Nicolas David Greber[6], Martin Grosjean[1]

1 University of Bern, Oeschger Centre for Climate Change Research & Institute of Geography, University of Bern, Bern, Switzerland

2 PAGES International Project Office, Bern, Switzerland

3 Centro de Ciencias Ambientales EULA-Chile, Universidad de Concepción, Concepción, Chile

4 SURF-EAWAG, Duebendorf, Switzerland

5 Geological Institute, ETH Zurich, Zurich, Switzerland

6 Institute of Geological Sciences, University of Bern, Bern, Switzerland

Corresponding author:

Julie Elbert
University of Bern
Institute of Geography & Oeschger Centre
Erlachstrasse 9a T3
3012 Bern, Switzerland
julie.elbert@giub.unibe.ch
Tel: + 41 (0) 31 631 5094

Abstract

Climate and environmental reconstructions from natural archives are important for the interpretation of current climatic change. Few quantitative high-resolution reconstructions exist for South America which is the only land mass extending from the tropics to the southern high latitudes at 56°S. We analysed sediment cores from two adjacent lakes in Northern Chilean Patagonia, Lago Castor (45°36'S, 71°47'W) and Laguna Escondida (45°31'S, 71°49'W). Radiometric dating (^{210}Pb, ^{137}Cs, ^{14}C-AMS) suggests that the cores reach back to c. 900 BC (Laguna Escondida) and c. 1900 BC (Lago Castor). Both lakes show similarities and reproducibility in sedimentation rate changes and tephra layer deposition. We found eight macroscopic tephras (0.2 - 5.5 cm thick) dated at 1950 BC, 1700 BC, at 300 BC, 50 BC, 90 AD, 160 AD, 400 AD and at 900 AD. These can be used as regional time-synchronous stratigraphic markers. The two thickest tephras represent known well-dated explosive eruptions of Hudson volcano around 1950 and 300 BC. Biogenic silica flux revealed in both lakes a climate signal and correlation with annual temperature reanalysis data (calibration 1900-2006 AD; Lago Castor r= 0.37; Laguna Escondida r= 0.42, seven years filtered data). We used a linear inverse regression plus scaling model for calibration and leave-one-out cross-validation (RMSEv = 0.56°C) to reconstruct sub decadal-scale temperature variability for Laguna Escondida back to AD 400. The lower part of the core from Laguna Escondida prior to AD 400 and the core of Lago Castor are strongly influenced by primary and secondary tephras and, therefore, not used for the temperature reconstruction. The temperature reconstruction from Laguna Escondida shows cold conditions in the 5th century (relative to the 20th century mean), warmer temperatures from AD 600 to AD 1150 and colder temperatures from AD 1200 to AD 1450. From AD 1450 to AD 1700 our reconstruction shows a period with stronger variability and on average higher values than the 20th century mean. Until AD 1900 the temperature values decrease but stay slightly above the 20th century mean. Most of the centennial-scale features are reproduced in the few other natural climate archives in the region. The early onset of cool conditions from c. AD 1200 onward seems to be confirmed for this region.

Keywords: Climate change, Paleoclimatology, Quaternary, Sedimentology, Tephra, South America

1. Introduction

To investigate climate and environmental changes over time periods longer than the instrumental era, quantitative high-resolution records from various natural climate archives around the world are fundamental (Hegerl et al., 2006; Hegerl and Russon, 2011). Lake sediments are an excellent archive to reconstruct long-term fluctuations of environmental conditions (e.g. Williamson et al., 2009). In contrast to North America and Europe relatively few quantitative paleoclimate data sets exist for South America. However, this continent is climatically of particular interest because it is the only large land mass extending from the tropics to the southern high latitudes and intersects the entire southern westerly wind belt between 40-55°S (Garreaud et al., 2009). Especially the climate of Chilean Patagonia is dominated by seasonal changes of the westerly winds and related changes in temperature and precipitation.

Regional differences in climatic changes are significant in this area: Villalba et al. (2003) report that temperature data from stations along the Pacific coast between 37 and 43°S are characterized by negative trends in mean annual temperature with a marked cooling period from 1950 to the mid-1970s. In contrast, a warming trend is observed in the southern stations (south of 46° S). A similar pattern is found in the tree-ring derived temperature composites from both regions.

Quantitative, near-annually resolved proxy records for South America are mostly based on tree rings, corals or ice cores (Villalba et al., 2009; Neukom et al., 2011) whereas only three lake sediment records fulfilled the quality requirements (calibrated, high resolution, precise chronology, continuity of record) for the comprehensive multi-proxy multi-site Southern Hemisphere reconstructions (Neukom and Gergis, 2012; von Gunten et al., 2009; Elbert et al., 2012). While most of these high-resolution paleotemperature records in South America

81 are relatively short (back to AD 1500 - 1600), only six of the selected records span beyond
82 AD 1000 and only one reaches beyond AD/BC 1 (Neukom and Gergis, 2012). Most of the
83 paleoclimate research in Patagonia deals with Late-Glacial and Holocene time scales that are
84 much coarser in the temporal resolution (e.g. Villa-Martinez et al., 2012; Lamy et al. 2010
85 and references therein).
86 In this study, we present a 1600-years long mean annual temperature reconstruction and a
87 detailed history of volcanism from two adjacent lakes in the foot zone east of the Andes in
88 northern Patagonia of Chile, Lago Castor (45°36'S, 71°47'W) and Laguna Escondida
89 (45°31'S, 71°49'W). We have chosen two lakes with similar catchment properties and
90 investigate with multiple short sediment cores reproducible and robust features of climatic
91 change. First we present the individual chronological frameworks for both lakes (^{210}Pb, ^{137}Cs
92 and ^{14}C). This enables us to corroborate independent ages of macroscopic tephras in both lake
93 sediment cores and, after stratigraphic and geochemical correlation, verify and improve the
94 final chronology that is used for the climate reconstruction with sediments from Laguna
95 Escondida. In the second part, we correlate a range of organic and inorganic lake sediment
96 proxies in both lakes against meteorological data (AD 1900 – 2006) and build a statistical
97 calibration model to predict annual temperatures for the past from the flux of biogenic Si
98 (bSi). BSi flux has shown to be the best predictor for temperature and yields consistent results
99 in both lakes for the calibration period suggesting that it contains a robust and reproducible
100 temperature signal. Finally, this calibration is used to reconstruct temperature variations at
101 sub-decadal scale back to AD 400.
102

103 ## 2. Regional setting

104 Lago Castor (45°36'S, 71°47'W) and Laguna Escondida (45°31'S, 71°49'W) are located in
105 the Aysén region of Chile about 20 km east of Coyhaique (Fig. 1). The area lies in the

106 Southern Volcanic Zone (SVZ; Parada et al., 2001) where volcanic activity is caused by
107 subduction processes (Gutiérrez et al., 2005). The geology in the catchment areas consists
108 mainly of Cretaceous volcanic rocks with an outcrop area of granites and granodiorites
109 between both lakes. The study site was covered with ice during the Last Glacial Maximum
110 (Glasser et al., 2008). In consequence, large areas consist of glacially scoured bedrock
111 whereby the lakes are located along geologic fault-lines running largely in parallel with the
112 glacial lineations and the Pleistocene ice flow direction (Glasser et al., 2009). The soils in the
113 catchment are classified as humic umbrisols (Dijkshoorn et al., 2005) with loamy sand to
114 loamy silt texture (Peralta et al., 1979).
115 Before AD 1900 the main vegetation consisted of Lenga beech (*Nothofagus pumilio)* and
116 Antarctic beech (*Nothofagus antarctica)* (Abarzua et al., 2004; Neves et al., 2008).
117 Climatically induced fires caused variations of the vegetation in the catchment in the early
118 and late Holocene (Kitzberger and Veblen, 2003). Both catchments underwent substantial
119 changes from AD 1900 onwards when the region was first settled. The city of Coyhaique was
120 founded in AD 1929. The catchments of the lakes were not influenced by industrial activity
121 (Urrutia et al., 2002). Large parts of the Aysén basin experienced deforestation from AD
122 1936-1956 and were reforested with pine monocultures in the late 20th century (Quintanilla,
123 2008).
124 Both Lago Castor and Laguna Escondida are glacio-tectonic lakes between 700 and 725 m
125 asl. Lago Castor is relatively large (4.26 km^2), 52 m deep and has a catchment area of
126 estimated 24.5 km^2 (Urrutia et al., 2002). It has numerous small inflows and a larger outflow
127 (Rio Pollux) that drains into Rio Simpson and, finally to the Aysén fjord. Lago Castor is a
128 polimictic (no stratification in summer; measurement January 2009), oligothrophic
129 (phosphate below detection limit <0.07 mg/l), neutral (pH 7.2) freshwater (80 µS/cm) lake.

Laguna Escondida is 23 m deep, smaller than Lago Castor (estimated area: 1.8 km^2) but has two basins. An inflow is draining into the North East basin and the outflow stream is located on the South West of the western basin. Laguna Escondida is an exorheic polimictic, oligothrophic (PO_4^{3-} <0.07 mg/l), neutral (pH 7.1) freshwater (83.2 µS/cm) lake.

The region has a temperate oceanic climate. Precipitation is mainly caused by westerly winds that peak in summer between 45-55°S and expand northwards but weaken in winter (Garreaud et al., 2009). Very strong zonal precipitation gradients are observed between the Andes and the Patagonian steppe to the East. The closest meteorological stations are Puerto Aysén (68 km), Coyhaique (20 km) and Balmaceda (43 km). The records are however short (< 50 years) and discontinuous. The CRU TS 3.0 reanalysis data set (Mitchell and Jones, 2005) shows for the grid cell of the study sites average annual temperatures of 5.5°C for the period AD 1900-2000. The correlation field analysis between the CRU TS 3.0 temperature record at the grid cell of the study site and the rest of the grid cells over South America (1900-2000 AD; Fig. 1) suggests significantly positive correlations between the study site and southern South America (36 – 56°S) except for a region between 46-49°S in Argentina (eastern Patagonia) that shows no significant correlation. This regional pattern is consistent with the modern temperature trends between western and eastern Patagonia observed by Falvey and Garreaud (2009).

3. Material and methods

3.1. Coring and sampling for analytical measurements

Two short cores from Lago Castor (CAS-09-1 and CAS-09-3) and four short cores from Laguna Escondida (eastern basin: ESC-09-1/2/5; western basin ESC-09-3) were taken in February 2009 with an UWITEC corer. For this study we selected cores from the proximal eastern basin near the deepest part of Laguna Escondida (9.8 m water depth; ESC-09-5) and

155 from the relatively gently sloping area at 22 m water depth in the distal part of Lago Castor
156 (CAS-09-1; Fig. 1). The cores were sealed and stored under dark and cold (4°C) conditions
157 prior to analysis. Before sampling, the short cores CAS-09-1 and ESC-09-5 were analyzed
158 with non-destructive scanning techniques (X-ray fluorescence XRF and in-situ reflectance
159 spectroscopy VIS-RS). All cores were stratigraphically correlated using tephra layers and
160 mm-scale scanning data. After scanning, one core half was sampled and freeze-dried for
161 analytical measurements. For Lago Castor the complete core CAS-09-1 was sampled at 2 mm
162 resolution except for the primary tephra layers that were deposited directly into the lake and
163 are not mixed with lake sediment. We sampled the core of Laguna Escondida at 1 mm
164 resolution. Larger samples (1-2 cm resolution) were taken from the primary tephra layers for
165 XRF analysis.
166 The upper 25 cm of the second half of ESC-09-5 and CAS-09-3 were sampled in 0.5 cm
167 resolution for ^{210}Pb, ^{226}Ra and ^{137}Cs activity measurements.
168
169 ***3.2. ^{210}Pb, ^{226}Ra, ^{137}Cs and ^{14}C measurements***
170 Gamma ray counts of ^{210}Pb (46.5 keV) and ^{137}Cs (662 keV) were collected for more than 20 h
171 using Canberra low background, well-type HPGe detectors. ^{226}Ra was determined by
172 measuring the activity of ^{214}Pb (352 keV) and ^{214}Bi (609 keV) in radioactive equilibrium.
173 In order to convert ^{210}Pb activity profiles into ages, we tested two numerical model types, the
174 Constant Initial Concentration (CIC) and the Constant Rate of Supply (CRS, Appleby, 2001)
175 model. For the core ESC-09-5, unsupported ^{210}Pb was calculated with the level-by-level
176 method from the ^{226}Ra activity (Appleby, 2001). For CAS-09-3, ^{226}Ra values were below
177 detection limit. Therefore, supported ^{210}Pb was considered to be zero (total ^{210}Pb =
178 $^{210}Pb_{unsupported}$).

179 In contrast to the CRS model, the CIC age model displayed several age inversions for both
180 cores and was therefore not pursued. ^{137}Cs measurements were used as independent time
181 markers to constrain the ^{210}Pb age models. ^{137}Cs fallout in southern Chile peaked in AD 1964
182 (Environmental Measurements Laboratory, 2008).
183 In the absence of terrestrial plant macrofossils in most parts of the sediment cores, AMS
184 radiocarbon measurements were performed on the total organic fraction of bulk sediment
185 samples. Such ^{14}C ages may potentially be affected by ^{14}C reservoir effects. For Lago Castor,
186 ^{14}C reservoir effects were assessed using a paired measurement on bulk organic fraction and
187 on a syndepositional terrestrial leaf macrofossil (CAS-09-1), which yielded identical ages.
188 For Laguna Escondida potential reservoir effects were evaluated and discarded by parallel
189 ^{14}C measurements of syndepositional diagnostic tephra layers which yielded similar ages in
190 both lakes (Castor and Escondida). ^{14}C measurements were performed either at the Poznan
191 Radiocarbon Laboratory, Poland, or at Beta Analytic Inc. All dates were calibrated using the
192 SHCal04 Southern Hemisphere Calibration curve (McCormac et al., 2004); the chronology
193 was made with the clam age modeling script of Blaauw (2010) using linear interpolation.
194 Furthermore, a distinct light tephra deposition in the core CAS-09-1 was identified as
195 eruptive material from the second major Holocene eruption of the Hudson volcano (H2, 3600
196 yr BP; Naranjo and Stern, 1998) and included in the age model as independent time marker.
197

198 ***3.3. Scanning methods (VIS-RS, XRF)***

199 Immediately after opening, all cores were analyzed with non-destructive scanning reflectance
200 spectroscopy in the visible range VIS-RS (380–730 nm; spectral resolution 10 nm, sample
201 resolution 2 mm) using a Gretag Mcbeth spectrophotometer. Reflectance spectra show
202 characteristic patterns and absorption bands holding information about organic compounds
203 (mainly photopigments; Rein and Sirocko, 2002; von Gunten et al., 2009) and the minerals

204 illite, chlorite and biotite (Rein et al., 2005; Trachsel et al., 2010). In this study we used the
205 relative absorption band depth centered between 660-670 nm ($RABD_{(660;670)}$) as a proxy for
206 organic material in the sediment (Rein and Sirocko, 2002; von Gunten et al., 2009) and the
207 reflectance ratio between 570 nm and 630 nm wavelength (i.e. the slope between 570 and 630
208 nm; R_{570}/R_{630}), as a proxy for the concentration of the lithogenic fraction (illite, chlorite and
209 biotite) in the sediments (Rein and Sirocko, 2002; Trachsel et al., 2010).
210 Additionally, the short cores CAS-09-1 and ESC-09-5 were analyzed with an AVAATECH
211 XRF Core Scanner that provided information about the elemental composition of the
212 sediments at a 0.2 mm measuring resolution. Al, Si, P, S, Cl, K, Ca, Ti, V, Cr, Mn, Fe were
213 measured at a tube voltage of 10 kV. The split sediment core surface was covered with a 4
214 µm thick *Ultralene SPEX CertiPrep*-foil to avoid contamination and desiccation of the
215 sediment. In the particular setting of the lake (i.e. in the absence of endogenic marl) we
216 interpreted the element Ca as an indicator for allochthonous lithoclastic material (mainly
217 plagioclase from tephra and eroded soils) and the element ratios Ca/Fe as an indicator for
218 pedogenic input (Koinig et al., 2003).
219
220 ***3.4. Analytical methods (C/N, biogenic silica, MAR and tephra)***
221 Total organic carbon (TOC) and total nitrogen (TN) were measured using a Vario Macro
222 Elemental Analyzer (Elementar Analysen Systeme) on freeze-dried carbonate-free sediment
223 material (100-200 mg). The C/N ratio can be used as a measure of the ratio between aquatic
224 and terrestrial sources of organic matter (Meyers and Teranes, 2001). If the C/N ratio
225 indicates that the primary source of sedimentary organic matter is aquatic ($C/N < 9$), TOC
226 and TN can be used as proxies for primary production in the lake.
227 Biogenic silica (bSi) concentration in the sediment was determined using alkaline leaching
228 (Mortlock and Froelich, 1989) and ICP-OES, and corrected for lithogenic Si according to

229 Ohlendorf and Sturm (2007). We applied an $Al:Si_{lithogenic}$ ^{wt}ratio of 1:3 as determined by XRF
230 for unweathered sedimentary volcanoclastic material from Lago Castor and Laguna
231 Escondida (data see Supplementary Tables 1 and 2).
232 The annual mass accumulation rate MAR (g cm^{-2} yr^{-1}) was calculated with the following
233 equation:
234 $MAR = dw / (1/2*\pi * r^2*i* a)$ (1)
235 dw = dry weight per sample (mg)
236 r = radius of core liner (cm)
237 i = sampling interval (cm)
238 a = years per sampling interval (yr/cm)
239
240 The bSi flux was calculated by multiplying the bSi concentrations (mg g^{-1}) with the mass
241 accumulation rate MAR (g cm^{-2} yr^{-1}).
242 Primary tephra deposits (deposited directly on the lake) were identified visually and with Ca
243 enrichments in the scanning XRF (AVAATECH XRF Core Scanner). Bulk tephra samples
244 were grinded, spiked with LiF and either melted to glass pills or compressed to powder pills
245 for the quantitative elemental analysis (Uniquant) with a XRF spectrometer (Philips PW
246 2400). The tephra layers of both lakes were dated with ^{14}C samples above or below the
247 tephras or by linear interpolation between two radiocarbon-dated points.
248
249 ***3.5. Climate data and climate reconstruction***
250 All sediment proxies in both lakes were compared with meteorological data from the CRU
251 TS 3.0 reanalysis data set (Mitchell and Jones, 2005; 0.5°x0.5° grid cell 45°S / 72°W). We
252 used the Pearson's product moment correlation coefficient r and corrected the related p-
253 values for autocorrelation ($p_{(aut)}$, Dawdy and Matalas, 1964) to test the correlations and

254 significance between the lake sediment proxies and the meteorological time series. For the
255 calibration with meteorological data (calibration-in-time) we used raw and seven years
256 triangular filtered data to account for chronological uncertainties in the calibration period and
257 to optimize the calibration (Koinig et al., 2002, von Gunten et al., 2012). The climate
258 inference model was calculated with the inverse regression plus scaling method. Split period
259 validation was performed using a calibration (AD 1900–1953) and validation (AD 1954–
260 2008) period. Leave-one-out cross-validation (jack knifing) was carried out on the entire
261 calibration period (AD 1900–2008) to calculate the root mean squared error of prediction
262 (RMSEP). Finally, temperature was reconstructed back to AD 400.
263 Because local meteorological data are short and discontinuous and cannot be used for
264 calibration purposes we considered the use of reanalysis data. To test the performance of the
265 CRU TS 3.0 data, we correlated the gridded data with the nearest station data of Balmaceda
266 (data 1963-1981, 1992-2008). Pearson correlation coefficients revealed a high correlation for
267 the period from AD 1963-1981 ($r = 0.79$, p-value<0.005) and for the period AD 1992-2008 (r
268 $= 0.8$, p-value<0.005). We also found high correlations for the reanalysis data with the station
269 of Puerto Aysén for the period AD 1953-1981 ($r = 0.70$, p-value<0.005). According to the
270 good performance, we used the reanalysis data for the calibration. As expected, temperature
271 and precipitation are negatively correlated ($r = -0.4$).
272

273 # 4. Results

274 ## *4.1. Lake sediment classification and tephras*

275 Both lakes contain at the coring sites (Fig. 1) three sediment facies:

276 I. Lake sediments are composed of brownish (Munsell color: Lago Castor: 10YR – 4/3;
277 Laguna Escondida: 10YR – 3/2) diatomaceous silt (Lago Castor: Median = 29.2 μm,
278 Laguna Escondida: Median = 23.4 μm) with medium to low concentrations of organic

matter (Lago Castor: TOC = 2-8%; Laguna Escondida: TOC = 5-11%). The only macrofossils found were a terrestrial leaf and a bivalve in Lago Castor. Inorganic carbonates are absent in the sediment.

II. Primary tephra layers are composed of blackish (Munsell color: GLEY 2 – 5PB) silt and sand (20-2000 μm) that were deposited as atmospheric fallout directly into the lake and are not mixed with lake sediments (Facies I). The tephra in Lago Castor at the bottom of the core (68 cm) is grayish-whitish (Munsell color: 5Y - 8/1).

III. The third facies is a mix between reworked tephra from the catchment and autochthonous lake sediments, typically subsequent to a primary tephra. The mixed facies are more abundant in Lago Castor while the tephra in Laguna Escondida are sharper confined and separated from Facies I.

The distribution of the sediment facies in both lakes is shown in Figs. 2a and 2b (and Fig. S1 and Table S1 supplementary material). For the regional tephra-chronological and stratigraphic core correlation the following tephras are most diagnostic: the grayish-white >2 cm thick T8 (CAS at 68-70 cm depth) tephra and the black 2 mm- thick T7 tephra (CAS at 65 cm) in lake Castor (the core ESC-09-5 does not extend to that depth), the 1-2 cm thick black T6 tephra (CAS at 48-49 cm; ESC at 66-68 cm); the cluster of 4 black tephras T2-5 within 15 cm of sediments (CAS at 42.5-28 cm; ESC at 59-44 cm) among which T3 (2-5 cm thick) is the most prominent one; the T2 tephra with its fine grains and distinct lighter (dark grey) color (CAS at 28.29 cm; ESC at 44-45 cm), and the very sharp black 3 mm tephra T1 (ESC at 30.5 cm; CAS at 23-24 cm). The base of T1 in core CAS-09-1 shows an erosional surface and a microfault suggesting that sediments are missing between CAS T1 and CAS T2. In comparison with the sediment strata in Laguna Escondida, the sediment hiatus between CAS T1 and T2 is approximately 10 cm.

The geochemical analysis of the four largest primary tephra (T3, T4, T6, and T8; supplementary material Table S1 and Fig. S2) shows that all the black tephra (T3, T4 and T6) are very similar in their elemental composition (medium to high K_2O calc-alkaline, SiO_2 50-64%) and relative abundances of macro and micro elements suggesting a similar source of the eruptions. The KO_2/SiO_2 and Zr/SiO_2 ratios of CAS-T8 are very similar to the eruption H2 of Hudson volcano dated to 3600 BP (calibrated BC 1947-1770; Supplementary Fig. S3; Naranjo and Stern, 1998) which is consistent with the extrapolated age of c. BC 1960 for CAS-T8 (Section 4.2.). According to the K_2O, SiO_2 and Zr diagrams (Supplementary Fig. S3) all of the four tephra (maybe except T3) belong to the realm of Holocene eruptions of Hudson Volcano situated 98 km to the southwest from the study site (after Naranjo et al., 1993; T3 might belong to one of the other SVZ volcanoes).

4.2. Chronology

Fig. 2 shows the age depth models as calculated with the constrained and unconstrained CRS models and the ^{14}C dates for Lago Castor and Laguna Escondida. The ^{14}C dates are listed in Table 1.

In Lago Castor, ^{137}Cs activity reaches the highest value at a core depth of 3.4 cm and is used as a time-marker to constrain the ^{210}Pb age model at this sediment depth to AD 1964. The ^{210}Pb profile shows in general a very low initial activity ($A_0 < 100$ Bq/kg) and, as a consequence substantial age uncertainties in the lower part of the profile despite extended counting times. However it shows generally decreasing values from the sediment surface towards larger depths and smaller age uncertainties between AD 1950-1960. The sedimentation rates as calculated from the CRS model (data not presented) show higher values between AD 1920 and AD 1963, and a trend towards lower values from AD 1970 to present. Fig. 2a (right panel) shows the combined age model for the entire core including the

329 ^{14}C dates. At 60.5 cm sediment depth both the total organic fraction of bulk sediment and a
330 syndepositional terrestrial leaf macrofossil are dated. Both fractions yield identical ages
331 (3125 ± 35 ^{14}C yr BP and 3100 ± 35 ^{14}C yr BP, respectively) suggesting that bulk sediment
332 TOC produces reliable ^{14}C ages and is not affected by ^{14}C reservoir effects in this lake. The
333 sediment hiatus as indicated by the erosional surface at 24 cm sediment (see section 4.1.)
334 depth is also confirmed by ^{14}C dates with a gap of c. 300 years between 23.5 and 24 cm
335 sediment depth. According to the age-depth model and allowing for ^{14}C dating uncertainties,
336 the tephras in Laguna Castor are dated to c. 1950 BC (T8, extrapolated), c. 1700 BC (T7), c.
337 300 BC (T6), c. 50 BC (T5), c. 90 AD (T4), c. 160 AD (T3), c. 400 AD (T2) and to between
338 800 - 1000 AD. The age of T8 matches precisely the age of the known Hudson tephra H2
339 (3600 BP uncalibrated; Naranjo and Stern 1998; calibrated 1900-2000 BC) and the age of T6
340 corresponds to the known Hudson 2200 BP tephra (uncalibrated; Naranjo and Stern 1998;
341 calibrated between 350 – 120 BC within a large ^{14}C plateau).
342 Fig. 2b shows the constrained and unconstrained CRS ^{210}Pb age-depth model for Laguna
343 Escondida. ^{137}Cs activity reaches maximum values at 4.25 cm depth. ^{210}Pb activities are also
344 generally very low but age uncertainties are much smaller than for Lago Castor. The late
345 Holocene chronology consists of three ^{14}C dates and five tephra ages (T2-T6) chrono-
346 stratigraphically correlated with Lago Castor. The uppermost tephra (T1, at 30 cm depth) is
347 ^{14}C dated to c. 950 AD.
348
349 ***4.3. Lake sediment proxies***
350 Fig. 3a summarizes the results of the proxies measured with scanning and analytical methods
351 for the Laguna Castor core CAS-09-1. The VIS-RS proxy $RABD_{(660;670)}$ show an increase
352 from the bottom of the core to 60 cm depth, a decrease to 30 cm depth and an increase
353 towards the top of the core. R_{570}/R_{630} (proxy for lithogenic concentration) is negatively

354 correlated to $RABD_{(660;670)}$ ($r= -0.63$, $p_{(aut)}<0.001$) and above average values for primary and
355 secondary tephra deposits. Total Ca shows very high values for the core sections with tephra
356 deposits and decreasing values towards the top of the core. The Ca/Fe ratios show similarities
357 with total Ca and peak in the tephra layers, and remain rather stable from 20 cm core depth
358 towards the top of the core.
359 C/N ratios show decreasing values from 20 cm towards the top of the core, while TOC is
360 increasing. In the lower part of the core, C/N ratios are highly variable at the centennial scale
361 ranging from more terrestrial sources of carbon (C/N ratio > 12-14) to more aquatic primary
362 production (C/N ratios < 10).
363 BSi concentrations show an increasing trend towards the top of the core and follow very
364 closely the TOC concentrations curve. Below 30 cm core depth, the record is interrupted by
365 many tephra layers. In contrast to bSi concentration values, bSi flux data show rather constant
366 values with minor fluctuations in the top 30 cm. BSi flux data are independent of matrix
367 effects and MAR changes (i.e. independent of variable admixtures of secondary volcanic
368 tephra material to the sediments) but rely strongly on the quality of the chronology. MAR is
369 inversely correlated with TOC (%) and bSi concentrations, ranges between 0.048 and 0.159
370 mg cm^2 yr^{-1} and shows a decreasing trend from 20 cm core depth upwards. Water content
371 shows a similar trend as TOC (%) and bSi (µg/g), and an inverse pattern compared to MAR.
372 This suggests that TOC and bSi concentrations are influenced by MAR and water content
373 and, ultimately by variable fluxes of lithogenic (volcanic) material.
374 Fig. 3b summarizes the results of the proxies measured for the short core in Laguna
375 Escondida ESC-09-5. These are essentially the same proxies as in Lago Castor. VIS-RS
376 proxies $RABD_{(660;670)}$ and R_{570}/R_{630} are negatively correlated ($r= -0.83$, $r^2=0.69$,
377 $p_{(aut)}=<0.001$). $RABD_{(660;670)}$ shows very low values while R_{570}/R_{630} shows high values in the
378 tephra layers. $RABD_{(660;670)}$ shows an increasing trend towards the top of the core. In contrast,

379 R_{570}/R_{630} is decreasing. Total Ca in ESC-09-5 shows a similar behavior as it was observed in
380 CAS-09-1: core sections with tephra deposits show high values. From 25 cm towards the top
381 of the core total Ca decreases. The Ca/Fe ratio shows similarities with total Ca and peaks in
382 the tephras, but remains very stable from c. 40 cm core depth (above tephra ESC-T2) to the
383 top of the core. This suggests that the composition of the lithogenic fraction in the lake
384 sediments remained stable for the past 1600 years (i.e. the length of our climate
385 reconstruction; see Section 4.4.).
386 In the uppermost 15 cm, C/N measurements suggest predominantly aquatic sources for the
387 organic matter (C/N < 9). C/N ratios decrease slightly towards the top of the core (as in CAS-
388 09-1) while TOC increases.
389 BSi (µg/g) shows a pattern similar to the measurements in CAS-09-1, but a weaker trend
390 towards the top of the core. For bSi flux, the long-term increasing trend of the bSi (µg/g) data
391 appears to be removed. This is attributed to the removed matrix effect, which in turn is
392 consistent with decreasing MAR and Ca (cps) values in the top part of the core. From 57 to
393 81 cm core depth bSi flux is on average significantly higher than for the upper part of the
394 core. MAR is on average higher than in CAS-09-1 and ranges between 0.08 and 0.52 mg cm^{-2}
395 yr^{-1}. Water content shows an increasing trend towards the top of the core and very low values
396 for tephra deposits.
397 In summary, all proxies show very similar trends in both lakes, suggesting that there is a
398 significant common signal of environmental change, and that the measurements are
399 reproducible. However, in comparison with Lago Castor, Laguna Escondida shows generally
400 a much clearer separation between Facies I and Facies II with sharp boundaries between the
401 tephras and the lake sediments. Lago Castor shows more sediment sections with mixed
402 facies. Thus we expect a better signal of climate change in the sediments of Laguna
403 Escondida than in those of Lago Castor.

404

405 ***4.4. Calibration and temperature reconstruction***

406 Fig. 4 shows the bSi flux data for both lakes in comparison with the meteorological mean
407 annual temperatures from AD 1900-2002. All three time series (7-yr filtered due to dating
408 uncertainties) show an increasing trend from AD 1900 to around AD 1940. A period of lower
409 values occurs around AD 1960 and a sharp increase is observed in the 1970s. From AD 1980
410 to AD 2002 the temperature time series show high values but a negative trend (cooling). The
411 bSi flux data from Lago Castor shows also maximum values but a negative trend only after
412 1990. In contrast bSi flux in Laguna Escondida shows a negative trend already from 1980
413 onwards, but slightly increases around 1990. In both lakes the bSi flux data show higher
414 (lower) values during the same time periods when CRU TS data show higher (lower)
415 temperature values, although the earlier peak (around AD 1937) in the data of Lago Castor is
416 not as pronounced as in the data of Laguna Escondida.
417 7-years filtered bSi flux data show the highest correlation with annual temperature data from
418 the CRU TS data set with a time lag of 6 years for Lago Castor ($r= 0.37$), and a time lag of 4
419 years for Laguna Escondida ($r= 0.42$). In both lakes, the lag applied (4-6 years) is smaller
420 than the $\pm 1\sigma$ dating uncertainty of the ^{210}Pb age model (Fig. 2).
421 Given the better correlation results, the smaller dating uncertainty in the calibration period
422 and the better separation of the sedimentary Facies we develop the calibration model and the
423 temperature reconstruction for Laguna Escondida. Calibration and validation using split
424 periods (calibration period AD 1900–1953; validation period AD 1954–2008) shows a
425 RMSEv of 0.56 °C. Leave-one-out cross-validation using the entire calibration period (AD
426 1900-2008) results in a RMSEP of 0.27 °C.
427 Using the calibration model we reconstruct annual temperature anomalies for Laguna
428 Escondida back to AD 400. We do not extend the reconstruction further back in time because

(i) ecosystem disturbance by tephras is significant prior to 400 AD, (ii) bSi flux is much higher and outside the range of the observations in the calibration period and (iii) the Ca/Fe ratios are variable suggesting that sedimentation regimes and also the composition of the lithogenic fraction has changed prior to 400 AD. Fig. 5 (bottom) shows the climate reconstruction for Laguna Escondida based on 7-years filtered bSi flux data. The record indicates pronounced (multi)decadal-scale variability and warm periods between AD 550 to AD 1200 (except AD 850-900) and cold periods between AD 400 to AD 500, around AD 850-900, and AD 1200 to AD 1450. From AD 1450 to AD 1700 the reconstructed temperature anomalies show a period with larger multidecadal variability and on average higher temperature than the 20th century mean. From AD 1700 until AD 1900 the temperature anomalies decrease but show higher values than the 20th century mean.

5. Discussion

5.1. Quality of the chronology

The ^{210}Pb age models in both lakes shows a plausible age depth distribution with consistent mid-points. In both lakes the ^{210}Pb activity is generally very low (A_0< 100-130 Bq/kg) and challenging to measure despite long counting times. The total absence of ^{226}Ra and supported ^{210}Pb in the profile of Lago Castor is unusual. This seems not to be an artifact since uranium concentrations (as a proxy for ^{234}U, the precursor of ^{226}Ra) in the sediments are also below XRF detection limits. The ^{210}Pb chronology with uncertainties in both lakes implies that the proxy-climate calibration in the instrumental period needs to be optimized and the data filtered (Koinig et al., 2002; von Gunten et al., 2012). In consequence of the dating uncertainties we had to apply a 7-years triangular filter for the proxy-climate calibration. This filter is relatively large and leads, in combination with pronounced bioturbation and low sedimentation rates to a very strong autocorrelation of the proxy time series in the sediments.

454 In consequence the number of fully independent observations (effective sample size) in the
455 calibration period (100 years) is reduced and it is very difficult to obtain statistically
456 significant correlations if the p-values are corrected for autocorrelation (von Gunten et al.,
457 2012, see also section 5.2.). With regard to the proxy-climate calibration it is important to
458 note that the ^{210}Pb chronologies in both lakes are not tuned and in their original, fully
459 independently calculated state. Indeed, as Fig. 4 shows, the correspondence between the
460 proxy data and the climate data could be substantially enhanced by tuning the chronology on
461 the order of a few years which is still much smaller than the ± 1 σ dating uncertainty of the
462 ^{210}Pb model.
463 In Lago Castor the mass accumulation rate MAR as calculated from the CRS ^{210}Pb age model
464 (data not shown) shows slightly higher rates between AD 1920 and AD 1963. This time
465 coincides largely with the reported deforestation AD 1936-1956. The trend towards lower
466 sedimentation from AD 1970 to the present could be attributed to reforestation of pine
467 monocultures in the Aysén basin in AD 1984 (Quintanilla, 2008). The same trend towards
468 lower sedimentation rates from AD 1980 to present was also observed in the age model of
469 Laguna Escondida and seems to be a reproducible regional feature.
470 In the general absence of terrestrial organic macrofossils we had to use bulk organic fractions
471 for ^{14}C dating. These ages may potentially be affected by ^{14}C reservoir effects. However, the
472 identical ^{14}C ages of the only terrestrial plant macrofossil we could find in the sediments of
473 Lago Castor and the age of syndepositional bulk organic carbon suggests that the bulk
474 fraction of organic C is not affected by ^{14}C reservoir effects in this lake and yields reliable
475 ages. This can be expected since carbonates are absent in the catchment geology and the
476 sediments are free of inorganic carbon. Absence of ^{14}C reservoir effects is also supported by
477 the observation that (i) the linear extrapolation of the three uppermost ^{14}C dates goes through
478 modern times (AD 2010), (ii) that the known and independently dated tephra around 3600 BP

(uncalibrated, tephra H2, Naranjo and Stern, 1998) matches precisely with the sediment age as extrapolated from the lowermost two ^{14}C ages, and (iii) that the chrono-stratigraphic position of the tephra T6 in CAS matches with the known and independently dated tephra around 2200 BP (uncalibrated, Naranjo and Stern, 1998). Age inversions are absent in the Lago Castor chronology and the inferred sedimentation rates are constant through time. Although we could not find a terrestrial macrofossil in the sediment core of Laguna Escondida for parallel dating, a number of observations makes ^{14}C reservoir effects on the bulk organic fraction highly unlikely: (i) extrapolation of the uppermost two ^{14}C samples goes through modern times, (ii) the independently dated known tephra at 2200 BP (uncalibrated, Naranjo and Stern,1998) matches with the ^{14}C inferred age of the tephra T6 in Laguna Escondida, and (iii) the similar ages of the tephras ESC T5 and ESC T2 as inferred from the chronostratigraphic correlation with the corresponding tephras in Lago Castor are identical (within the ^{14}C dating uncertainty) with the ages as inferred from the ESC ^{14}C chronology.

The ^{14}C chronologies of the late Holocene can be regarded as reliable in both lakes. They yield ages for the eight tephras identified (within the ^{14}C dating uncertainty) and a good chronological framework for the late Holocene climate reconstruction.

5.2. Proxy-climate calibration, temperature reconstruction and regional paleoclimates from Patagonia

The correlation matrix between the multi-proxy data in both lakes and the climate data revealed that biogenic silica bSi flux contains a consistent signal for annual temperatures. Assuming that bSi flux to the sediments is mainly driven by diatom productivity it is suggested that temperature influences (diatom) primary production in these lakes. Similar results have been found in lakes around the world for temperature changes at very long

timescales (>10^5 years) in Lake Baikal (Russia) or Lake Biwa (Japan) (Colman et al., 1995; Xiao et al., 1997) and at interannual to millennial scales in the Arctic and Alps (McKay et al., 2008; Blass et al., 2007).

The very similar pattern of bSi flux changes in Laguna Escondida and adjacent Lago Castor further suggests that both bSi records are driven by a common regional factor (i.e. temperature) and that the results are reproducible. BSi in Laguna Escondida shows better results as compared to Lago Castor because Laguna Escondida is less likely affected by detrital secondary tephra material, which makes MAR and bSi flux calculations more difficult. In view of the dating uncertainties in the calibration period we have used 7-years triangular filtered data for calibration and reconstruction to optimize the calibration for all the different interdependent and counteracting effects (correlation coefficient, degrees of freedom, significance, RE and RMSEP; von Gunten et al., 2012).

For Laguna Escondida the calibration model reveals a RMSE of 0.56 °C (RMSEP = 0.27 °C) for the reconstruction of annual temperatures. This is about 5 (10) times smaller than the average amplitude of decadal scale temperature variability (Fig. 5) showing that most of the reconstructed temperature variability during the last 1600 years represents significant climatic changes.

Our record shows relatively warm temperatures from c. AD 550 to AD 1150, interrupted by a cold episode in the 9th century, and generally lower temperatures in the 5th century and from AD 1200 to AD 1450. Large multidecadal variability is found from AD 1450 to AD 1700 with three distinct warm peaks around AD 1480, AD 1580 and AD 1680. From AD 1700 until around AD 1900 (minimum AD 1910) the reconstruction shows decadal-scale fluctuations and generally decreasing temperatures but on average higher than the 20th century mean.

528 Comparing the temperature record of Laguna Escondida with other regional records is
529 challenging. Indeed, it appears from the spatial correlation map of the 20th century
530 temperature data (Fig. 1) that the spatial coherency pattern of temperature in Patagonia is
531 very complex with strong subregional gradients. The correlation decays particularly rapidly
532 towards the east (Argentinean Patagonia) and it is not clear whether or not the spatial
533 teleconnections of temperature remained stable through time with different combinations of
534 forcings and internal variability (Wilmes et al., 2012) or how the 20th century spatial pattern
535 represents centennial-scale variability. Villalba et al. (1997) have shown that the strong
536 regional heterogeneity of temperature in Northern and Southern Patagonia existed also for the
537 last 400 years, whereby the two adjacent areas show a very different structure of temperature
538 evolution. The second problem is that there are only a few regional (i.e. southern South
539 America) natural climate archives available, most of them showing a precipitation or a mixed
540 signal (mostly precipitation, temperature and sometimes wind; Villalba et al., 2009, Boucher
541 et al., 2011), or relatively poor (multidecadal) temporal resolution. It should also be noted
542 that the most recent comprehensive multiproxy and multi-site summer temperature field
543 reconstruction for southern South America (Neukom et al., 2011) does not have any regional
544 predictor for Patagonia prior to c. AD 1650 and the structure of summer temperature
545 (Neukom et al. 2011) and annual temperature (Laguna Escondida) variability is very different
546 at times. Thus it is not readily obvious what one would expect comparing the record of
547 Laguna Escondida with other existing records from that part of the world. However, our
548 Laguna Escondida record shares a number of distinct features with the Neukom et al. (2011)
549 reconstruction such as the warmth in the 10th and 11th centuries, warm peaks in the 14th
550 century, maximum cold between AD 1380 and 1460, and the distinct warmth around AD
551 1800 followed by cooling that culminated around AD 1900.

552 The sustained warmth between AD 900 and 1150 is supported by several findings in South
553 Patagonian lake sediment records (Fey et al., 2009; Moy et al., 2009) and the absence of
554 glacier advances (Masiokas et al., 2009). The Laguna Escondida record shows a very early
555 onset of generally very cool conditions (from AD 1230 onwards) which lasted, with some
556 interruptions through AD 1460. This is consistent with two glacier advances in the Northern
557 Patagonian Icefield (i.e. the nearest glaciers to Laguna Escondida) in the 13th and 14th
558 centuries (Masiokas et al., 2009). Interestingly there is no evidence for both advances from
559 glaciers further to the North in the North Patagonian Andes (35-42°S) and to the South in the
560 Southern Patagonian Icefield (49-50°S; Masiokas et al., 2009). The different temporal
561 structure of glacier advances in the three areas points again to the pronounced differences in
562 the regional climate. The early onset of cool and wet conditions at the beginning of the 13th
563 century has also been observed in Lago Cardiel, Argentina, by Stine (1994).
564 The three pronounced decadal-long warm periods with the high amplitudes between AD 1480
565 and 1680 seem enigmatic and are not present in the Neukom et al. (2011) summer
566 temperature reconstruction. However, these positive anomalies seem to be a regional feature.
567 Lago Guanaco in southern Patagonia (Moy et al., 2009) shows at least two short-lived high-
568 amplitude hydroclimatic changes during this period while lakes further to the east show
569 pronounced warmth for about one century after AD 1650. A distinct positive anomaly around
570 AD 1680 was also found in tree rings of Southern Patagonia (Villalba et al., 2003).
571 Only a few records reach back to AD 400. The cold 5th century as reconstructed from Laguna
572 Escondida has also been found in Laguna Las Viszcachas (51°S; Fey et al., 2009). Also the
573 persistently warm but variable period from c. AD 600 until c. AD 1100 has been found in
574 Laguna Las Viszcachas (Fey et al., 2009).
575 We also compared our qualitative data from the entire Laguna Escondida record (back to c.
576 900 BC) to the Late Holocene trends of the alkenone-based sea surface temperature data at

577 41°S from the Chilean margin (ODP Site 1233; Lamy et al., 2010). Both records show a
578 cooling trend over the past c. 4000 years, but the sample resolution in the marine cores is
579 relatively coarse (one data point per 200- 400 years).
580

581 ## 5 Conclusion

582 We have investigated late Holocene ^{210}Pb and ^{14}C dated sediments from two paired lakes in
583 northern Patagonia to explore the potential of the lake sediments for high-resolution
584 paleoclimate reconstructions and as archives for past volcanic activity.
585 The comparison of both lakes suggests that the eight identified tephras spanning from BC
586 1900 (T8) to AD 900 (T1) provide a robust chrono-stratigraphic framework and
587 tephrachronology that can be used for further paleoenvironmental studies in this area. The
588 eight tephras are dated to c. 1950 BC, c. 1700 BC, at c. 300 BC, c. 50 BC, c. 90 AD, c. 160
589 AD, c. 400 AD and at c. 900 AD.
590 Despite inherent dating difficulties for young sediments with very low initial ^{210}Pb activities
591 and corresponding age uncertainties, we found in both lakes that bSi flux responds sensitively
592 to annual temperatures during the calibration period (AD 1900 – 2006). This result has been
593 developed independently for both lakes suggesting that bSi flux contains a reproducible and
594 robust signal for annual temperatures.
595 The proxy-climate calibration model has been validated and used to reconstruct subdecadal-
596 scale temperatures for the past 1600 years back to AD 400. Most of the reconstructed
597 temperatures are within the calibration range. The cool 5th century was followed by warmer
598 temperatures between AD 600 and AD 1150. Rapid cooling started around AD 1200 and
599 persisted through AD 1450. Highly variable conditions with pronounced multidecadal
600 temperature amplitudes and peak warmth around AD 1480, AD 1560 and AD 1680 were
601 followed by cooling that culminated around AD 1900.

602 Our record compares well with the multi-decadal temperature variability documented in the
603 few paleo-temperature archives available in southern South America. However, the spatial
604 variability of 20th century temperatures, particularly the enigmatic observed subregional
605 cooling in the 2nd half of the 20th century points to the importance of regional climatic
606 heterogeneities that are still insufficiently resolved in the available paleo-temperature data
607 sets and dynamically not understood.
608
609 **Acknowledgements**
610 Marcela Espinoza of DIFROL kindly granted research permissions during fieldwork in Chile.
611 This research was supported by the Swiss National Science Foundation (NF-200020-121869)
612 and the Chilean Swiss Joint Research Programme (Grant CJRP 1001 and CONICYT SER-
613 001). We thank Sebastian Bertrand and an anonymous reviewer for thoughtful comments on
614 the manuscript.
615
616
617 **References**
618 Abarzua, A. M., Villagran, C., Moreno, P.I., 2004. Deglacial and postglacial climate history
619 in east-central Isla Grande de Chiloe, southern Chile (43°S). Quat. Res. 62, 49-59.
620 Appleby, P., 2001. Chronostratigraphic techniques in recent sediments, in: Last, W.M., Smol,
621 J.P. (Eds), Tracking Environmental Change Using Lake Sediments, Volume 1: Basin
622 Analysis, Coring, and Chronological Techniques. Dordrecht: Kluwer Academic
623 Publishers, pp. 171-201.
624 Araneda, A., Torrejón, F., Aguayo, M., Torres, L., Cruces, F., Cisternas, M., 2007. Historical
625 records of San Rafael glacier advances (North Patagonian Icefield): Another clue to 'Little
626 Ice Age' timing in southern Chile? Holocene 17, 987-998.

627 Blass, A., Bigler, C., Grosjean, M., Sturm, M., 2007. Decadal-scale autumn temperature
628 reconstruction back to AD 1580 inferred from the varved sediments of Lake Silvaplana
629 (southeastern Swiss Alps). Quat. Res. 68, 184-195.
630 Blaauw, M., 2010. Methods and code for 'classical' age-modelling of radiocarbon sequences.
631 Quat. Geochronol. 5, 512-518.
632 Boucher, É., Guiot, J., Chapron, E. 2011. A millennial multi-proxy reconstruction of summer
633 PDSI for Southern South America. Clim. Past. 7, 957–974.
634 Colman, S.M., Peck, J.A., Karabanov, E.B., Carter, J.S., Bradbury, J.P., King J.W., Williams
635 D.F., 1995. Continental climate response to orbital forcing from biogenic silica records in
636 Lake Baikal. Nature 378, 769-771.
637 Dawdy, D., Matalas, N., 1964. Statistical and probability analysis of hydrologic data, part III:
638 Analysis of variance, covariance and time series, in: Chow V.T. (Ed.) Handbook of
639 Applied Hydrology. McGraw-Hill Book Company, 8.68-8.90.
640 Dijkshoorn, J. A., Huting, J.R.M., Tempel, P., 2005. Update of the 1:5 million Soil and
641 Terrain Database for Latin America and the Caribbean (SOTERLAC; version 2.0). Tech.
642 Rep. 2005/01. ISRIC - World Soil Information, Wageningen
643 Elbert J., Grosjean M., von Gunten L., Urrutia R., Fischer D., Wartenburger R., Ariztegui D.,
644 Fujak M., 2012. Quantitative high-resolution winter (JJA) precipitation reconstruction
645 from varved sediments of Lago Plomo 47°S, Patagonian Andes, AD 1530-2001. Holocene
646 22, 460-469.
647 Environmental Measurements Laboratory, 2008. SASP Measurements Database. U.S.
648 Department of Homeland Security.
649 Falvey, M., Garreaud, R.D., 2009. Regional cooling in a warming world: Recent temperature
650 trends in the southeast Pacific and along the west coast of subtropical South America
651 (1979-2006). J. Geophys. Res. 114, D04102.

652 Fey, M., Korr, C., Maidana, N.I., Carrevedo, M.L., Corbella, H., Dietrich, S., Haberzettl, T.,
653 Kuhn, G., Lücke, A., Mayr, C., Ohlendorf, C., Paez, M., Quintana, F., Schäbitz, F.,
654 Zolitschka, B., 2009. Palaeoenvironmental changes during the last 1600 years inferred
655 from the sediment record of a cirque lake in southern Patagonia (Laguna Las Vizcachas,
656 Argentina). Palaeogeogr., Palaeoclimatol., Palaeoecol. 281, 363–375.
657 Garreaud, R.D., Vuille, M., Compagnucci, R. and Marengo, J., 2009. Present-day South
658 American climate. Palaeogeogr., Palaeoclimatol., Palaeoecol. 281, 180-195.
659 Glasser N.F., Harrison S., Jansson K.N., Kleman J., 2008. The glacial geomorphology and
660 Pleistocene history of southern South America between 38°S and 56°S. Quat. Sci. Rev. 27,
661 365-390.
662 Glasser N.F., Harrison S., Jansson K.N., 2009. Topographic controls on glacier sediment-
663 landform associations around temperate North Patagonian Icefield. Quat. Sci. Rev. 28,
664 2817-2832.
665 Gutiérrez, F., Gioncada, A., González Ferran, O., Lahsen, A., Mazzuoli, R., 2005. The
666 Hudson Volcano and surrounding monogenetic centres (Chilean Patagonia): An example
667 of volcanism associated with ridge-trench collision environment. J. Volcanol. Geoth. Res.
668 145, 207-233.
669 Hegerl G.C., Crowley T.J., Hyde W.T., Frame D.J., 2006. Climate sensitivity constrained by
670 temperature reconstructions over the past seven centuries. Nature 440, 1029-1032.
671 Hegerl,G.C., Russon, T., 2011. Using the Past to Predict the Future? Science 334, 1360-1361.
672 Kitzberger, T., Veblen, T.T., 2003. Influences of Climate on Fire in Northern Patagonia,
673 Argentina, in: Veblen, T.T., Baker, W.L., Montenegro, G., Swetnam, T.W. (Eds) Fire
674 Regimes and Climatic Change in Temperate Ecosystems of the Western Americas.
675 Springer-Verlag, New York, 296-321.

676 Koining, K.A., Kamenik, C., Schmidt, R., Augusti-Panareda, A., Appleby, P.G., Lami, A.,
677 Prazakova, M., Rose, N., Schnell, Ø.A., Tessadri, R., Thompson R., Psenner, R., 2002.
678 Environmental changes in an alpine lake (Gossenkollesee, Austria) over the last two
679 centuries – The influence of air temperature on biological parameters. J. Paleolim. 28,
680 147–160.
681 Koinig, K.A., Shotyk, W., Lotter, A.F., Ohlendorf, C., Sturm, M., 2003. 9000 years of
682 geochemical evolution of lithogenic major and trace elements in the sediment of an alpine
683 lake – the role of climate, vegetation, and land-use history. J. Paleolim. 30, 307-320.
684 Lamy, F., Kilian, R., Arz, H.W., Froncois, J-P., Kaiser, J., Prange M., Steinke T., 2010.
685 Holocene changes in the position and intensity of the southern westerly wind belt. Nature
686 Geosci. 3, 695-699.
687 Masiokas H.M., Rivera A., Espizua L.E., Villalba R., Delgado S., Aravena J.C., 2009.
688 Glacier fluctuations in extratropical South America during the past 1000 years.
689 Palaeogeogr., Palaeoclimatol., Palaeoecol. 281, 242–268.
690 McCormac, F.G., Hogg, A.G., Blackwell, P.G., Buck, C.E., Higham, T.F.G., Reimer, P.J.,
691 2004. SHCal04 Southern Hemisphere calibration, 0-11.0 cal. kyr BP. Radiocarbon 64,
692 1087-1092.
693 McKay, N. P., Kaufman, D. S., Michelutti, N., 2008. Biogenic silica concentration as a high-
694 resolution, quantitative temperature proxy at Hallet Lake, south-central Alaska, Geophys.
695 Res. Lett. 35, L05709.
696 Meyers, P.A., Teranes, J.L., 2001. Sediment organic matter, in: Last, W.M., Smol, J.P. (Eds.),
697 Tracking environmental change using lake sediments. Volume 2: Physical geochemical
698 methods. Kluwer Academic Publishers, Dordrecht, pp. 239-269.
699 Mitchell, T.D., Jones, P.D., 2005. An improved method of constructing a database of monthly
700 climate observations and associated high-resolution grids. Int. J. Climatol. 25, 693-712.

Mortlock, R., Froelich, P., 1989. A simple method for the rapid determination of biogenic opal in pelagic marine sediments. Deep-Sea Research 36, 1415-1426.

Moy C.M., Moreno P.I., Dunbar R.B., Kaplan M.R., Francois J.P., Villalba R., Haberzettl, T., 2009. Climate change in southern South America during the last two millennia, in: Vimeux F. et al. (Eds.) Past Climate Variability in South America and Surrounding Regions. New York: Springer, pp. 353–393.

Naranjo, J.A., Moreno, H., Banks, N.G., l993. La erupción del volcán Hudson en l991 (46°S), Región XI, Aisén, Chile. Serv. Nac. Geol. Minería Boletin 44, 1–50.

Naranjo, J. A., Stern, C.R., 1998. Holocene explosive activity of Hudson Volcano, southern Andes. B.Volcanol. 59/4, 291-306.

Neukom, R., Luterbacher, J., Villalba, R., Küttel, M., Frank, D., Jones, P.D., Grosjean, M., Wanner, H., Aravena, J.-C., Black, D., Christie, D., D'Arrigo, R., Lara, A., Morales, M., Soliz-Gamboa, C., Srur, A., Urrutia, R., von Gunten, L., 2011. Multiproxy summer and winter surface air temperature field reconstructions for southern South America covering the past centuries. Clim. Dyn. 37, 35-51.

Neukom, R., Gergis, J., 2012. Southern Hemisphere high-resolution palaeoclimate records of the last 2000 years. Holocene 22, 501–524.

Neves, R., Baretta, J., Mateus, M., 2008. Perspectives on integrated coastal zone management in South America. Lisboa (Portugal). IST Press.

Ohlendorf, C., Sturm, M., 2007. A modified method for biogenic silica determination. J. Paleolim. 39, 137-142.

Parada, M. A., Lahsen, A., Palacios, C., 2001. Ages and geochemistry of Mesozoic-Eocene back-arc volcanic rocks in the Aysén region of the Patagonian Andes, Chile. Rev. Geol. Chile 28, 25-46.

725 Peralta, M., Gonzalez, S., Carpinelli, A., Kühne, A., 1979. Suelos y erosión, in: Iren Corfo
726 (Eds.) Perspectivas de desarrollo de los recursos de la Región Aysén del General Carlos
727 Ibañez del Campo.
728 Quintanilla, V., 2008. Estado de recuperación del bosque nativo en una cuenca
729 Nordpatagonica de Chile, perturbada por grandes fuegos acaecidos 50 años atrás (44°-
730 45°S). Rev. Geogr. Norte Grande 39, 73-92.
731 Rein B., Sirocko F., 2002. In-situ reflectance spectroscopy - Analysing techniques for high-
732 resolution pigment logging in sediment cores. Int. J. Earth Sci. 91, 950-954. Erratum 2003.
733 Int. J. Earth Sci. 92, 143.
734 Rein B., Lueckge A., Reinhardt L., Sirocko F., Wolf A., Dullo W., 2005. El Niño variability
735 off Peru during the last 20,000 years. Paleoceanography 20, PA 4003.
736 Stine, S. 1994. Extreme and persistent drought in California and Patagonia during medieval
737 time. Nature 369, 546-549.
738 Trachsel, M., Grosjean, M., Schnyder, D., Kamenik, C., Rein, B., 2010. Scanning reflectance
739 spectroscopy (380–730 nm): A novel method for quantitative high-resolution climate
740 reconstructions from minerogenic lake sediments. J. Paleolim. 44, 979-994.
741 Urrutia, R., Yevenes, M., Barra, R., 2002. Determinación de los niveles basales de metales
742 traza en sedimentos de tres lagos andinos de Chile: lagos Chungará, Laja y Castor. Bol.
743 Soc. Chil. Quim. 47, 457-467.
744 Villa-Martínez, R., Moreno, P.I., Valenzuela, M.A., 2012. Deglacial and postglacial
745 vegetation changes on the eastern slopes of the central Patagonian Andes (47°S). Quat.
746 Sci. Rev. 32, 86-99.
747 Villalba, R., Boninsegna, J.A., Veblen, T.T., Schmelter, A., Rubulis, S., 1997. Recent trends
748 in tree-ring records from high elevation sites in the Andes of northern Patagonia. Climatic
749 Change 36, 425–454.

Villalba, R., Lara, A., Boninsegna, J.A., Masiokas, M., Delgado, S., Aravena, J.C., Roig, F.A., Schmelter, A., Wolodarsky, A., Ripalta, A., 2003. Large-scale temperature changes across the southern Andes: 20th century variations in the context of the past 400 years. Climatic Change 59, 177-232.

Villalba, R., Grosjean, M., Kiefer, T., 2009. Long-term multi-proxy climate reconstructions and dynamics in South America (LOTRED-SA): State of the art and perspectives. Palaeogeogr., Palaeoclimatol., Palaeoecol. 281, 175–179.

von Gunten, L., Grosjean, M., Rein, B., Urrutia, R., Appleby, P., 2009. A quantitative high-resolution summer temperature reconstruction based on sedimentary pigments from Laguna Aculeo, central Chile, back to AD 850. Holocene 19, 873-881.

von Gunten, L., Grosjean, M., Kamenik, C., Fujak, M., Urrutia, R., 2012. Calibration of bio-geochemical and physical proxies from non-varved lake sediments with climate data: methodology and case studies. J. Paleolim. 47, 583-600.

Williamson, C.E., Saros, J.E., Vincent, W.F., Smol J.P., 2009. Lakes and reservoirs as sentinels, integrators, and regulators of climate change. Limnol. Oceanogr. 54, 2273-2282.

Wilmes, S.B., Raible, C.C., Stocker, T.F., 2012. Climate variability of the mid- and high-latitudes of the Southern Hemisphere in ensemble simulations from 1500 to 2000 AD. Clim. Past Discuss., 7, 3091-3129.

Xiao, J., Inouchi, Y., Kumai, H., Yoshikawa, S., Kono Y., Liu, T., An, Z., 1997. Biogenic Silica record in Lake Biwa of central Japan over the past 145,000 years. Quat. Res. 47, 277-283.

Table Captions:

Table 1: Samples and radiocarbon ages for Lago Castor and Laguna Escondida. The calibration was made with the SHCal04 Southern Hemisphere Calibration curve (McCormac et al., 2004).

Figure captions:

Fig.1: Left: Map of southern South America and location of the study sites (modified from Araneda et al., 2007). Top center: bathymetry of Laguna Escondida and location of the two different coring sites. Bottom center: bathymetry of Lago Castor and coring site. Right: spatial correlation map (top) and related p-value (bottom) for annual temperature between our study site (arrow and white square) and the rest of South America (see method section for details).

Fig. 2a) ^{137}Cs, ^{226}Ra and ^{210}Pb activity profiles (2 sigma error of the measurements), and ^{210}Pb age models with dating uncertainty for Lago Castor. The Figure to the right shows the combined ^{210}Pb and ^{14}C age-model for the entire core calculated with the ^{14}C clam model (Blaauw, 2010) and the ages of the tephra CAS T1 – T8. b) shows the same for Laguna Escondida.

Fig. 3: Relative Absorption Band Depth centered between 660-670 nm ($RABD_{(660;670)}$ indicative of total chlorin, and spectral index R_{570}/R_{630} (indicative of lithogenic concentration) derived from VIS-RS, scanning XRF data for Ca and Ca/Fe, C/N mass ratio and TOC, biogenic silica concentration and flux rates, MAR and water content of (a) Lago Castor and (b) Laguna Escondida.

Fig. 4: Mean annual temperature for the study area (grid cell 45.5–44.5°S and 72.5–71.5°W; CRU TS 3.0, 7-years triangular filtered; top), 7-years filtered bSi flux data for Lago Castor (middle) and Laguna Escondida (bottom).

Fig. 5: Reconstructed annual temperature anomalies (wrt 20th century mean) derived from bSi flux data from Laguna Escondida. The thick black line represents 7-year smoothed temperature data used for calibration (CRU TS 3.0, AD 1900-2006). The thin black line represents the reconstructed temperature with the corresponding upper and lower 95% confidence interval. The dashed line shows the 30 years running mean. Inset: 30-year filtered summer and winter multi-proxy temperature reconstructions for southern South America by Neukom et al. (2011). Colors denote different regions of southern South America.

Supplementary Material

Supplementary Table S1: Stratigraphic position, thickness and age of the tephras T1 to T8 in Laguna Escondida and Lago Castor with dating uncertainty.

Supplementary Table S2: Chemical compositions (in wt %) of tephra samples T3, T4, T6 and T8 in Laguna Escondida and Lago Castor. Asterisks denote replicates.

Supplementary Fig. S1: Photographs of the cores CAS-09-1 (21.5 m water depth) and ESC-09-5e (9.8 m water depth) and tephras T1 to T8.

Supplementary Fig. S2: Elemental ratios of the tephras T3, T4, T6 and T8 in Laguna Escondida and Lago Castor.

Supplementary Fig. S3: SiO_2 vs K_2O and Zr for the tephra samples T3, T4, T6 and T8 from Lago Castor (red bold asterisks, this study) and Laguna Escondida (red asterisks, this study) compared with the three known Holocene tephras from Hudson volcano (black data, Naranjo and Stern, 1998): crosses denote samples of lava, solid circles denote bulk pumice for the 6700-, 3600-, and the 2200-BP eruptions and other eruptions (open circles) from Hudson Volcano compared with samples from other volcanoes in the Southern Volcanic Zone SSVZ (Maca, Cay, Mentolat, and Melimoyu) and in the Austral Volcanic Zone (AVZ). Solid squares show tephras from Los Toldos, Argentina, and Tierra del Fuego assigned to the 3600- and 6700-BP eruption of Hudson Volcano.

Figure1

Click here to download high resolution image

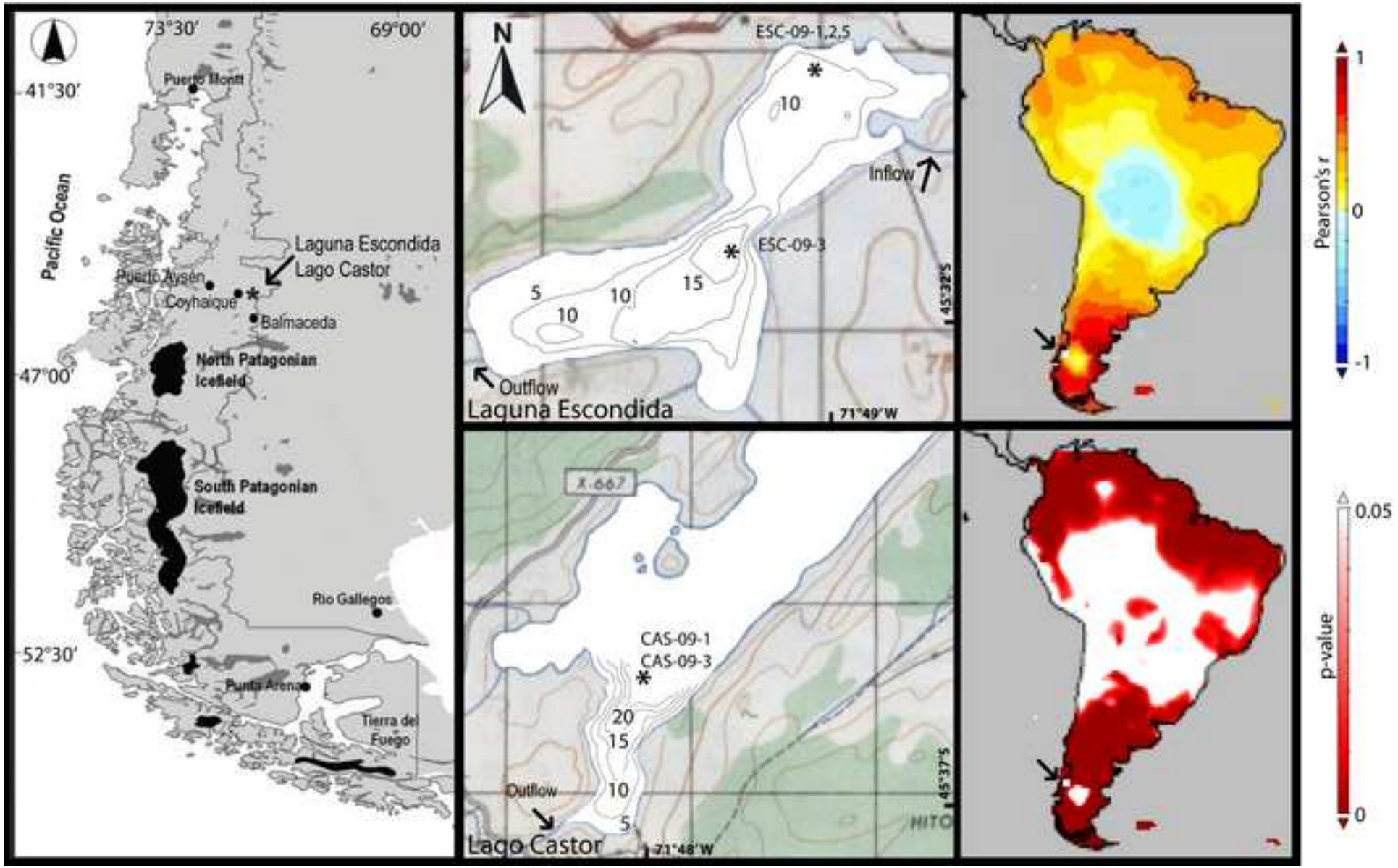

Figure2

Click here to download high resolution image

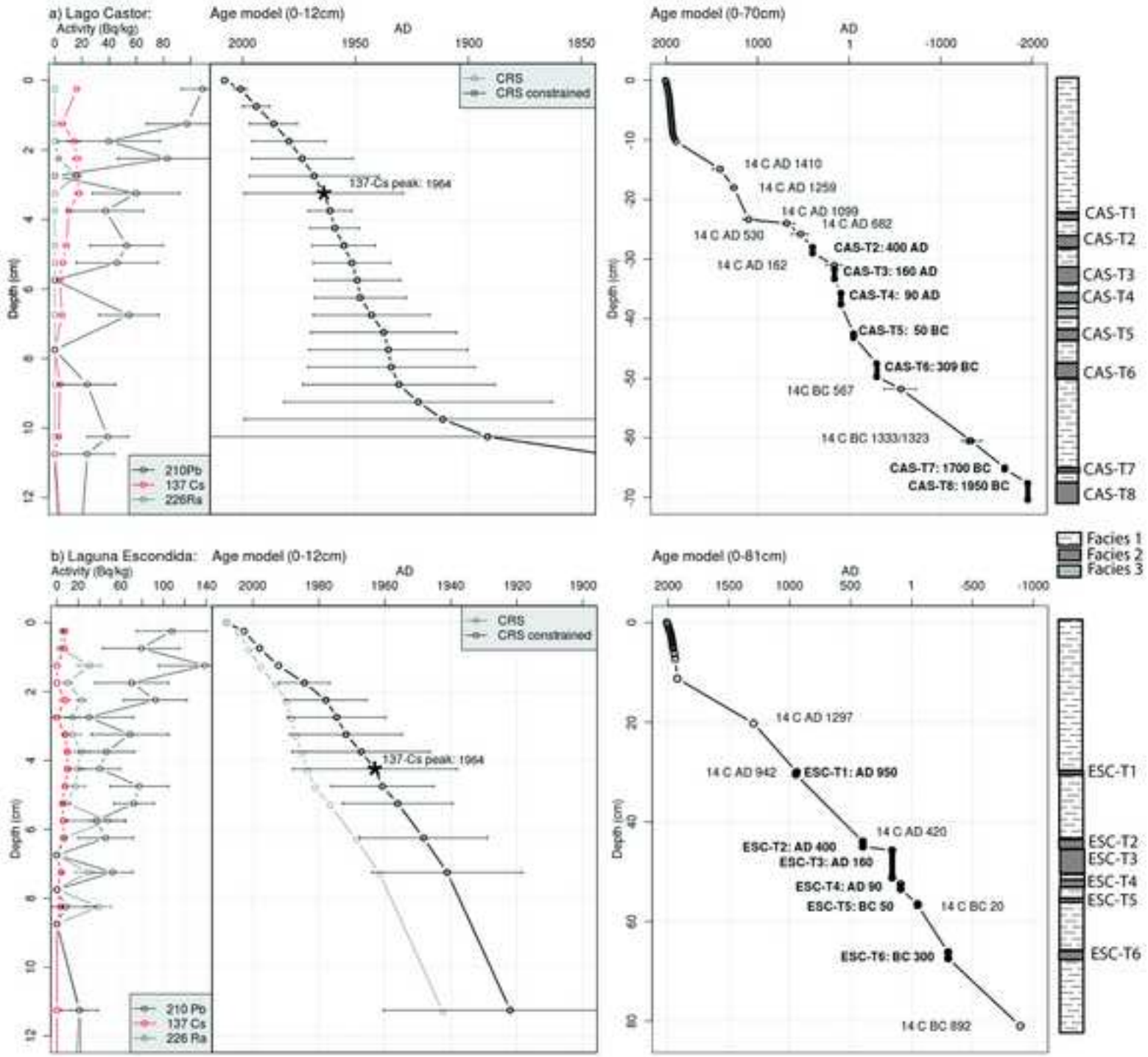

Figure3

Click here to download high resolution image

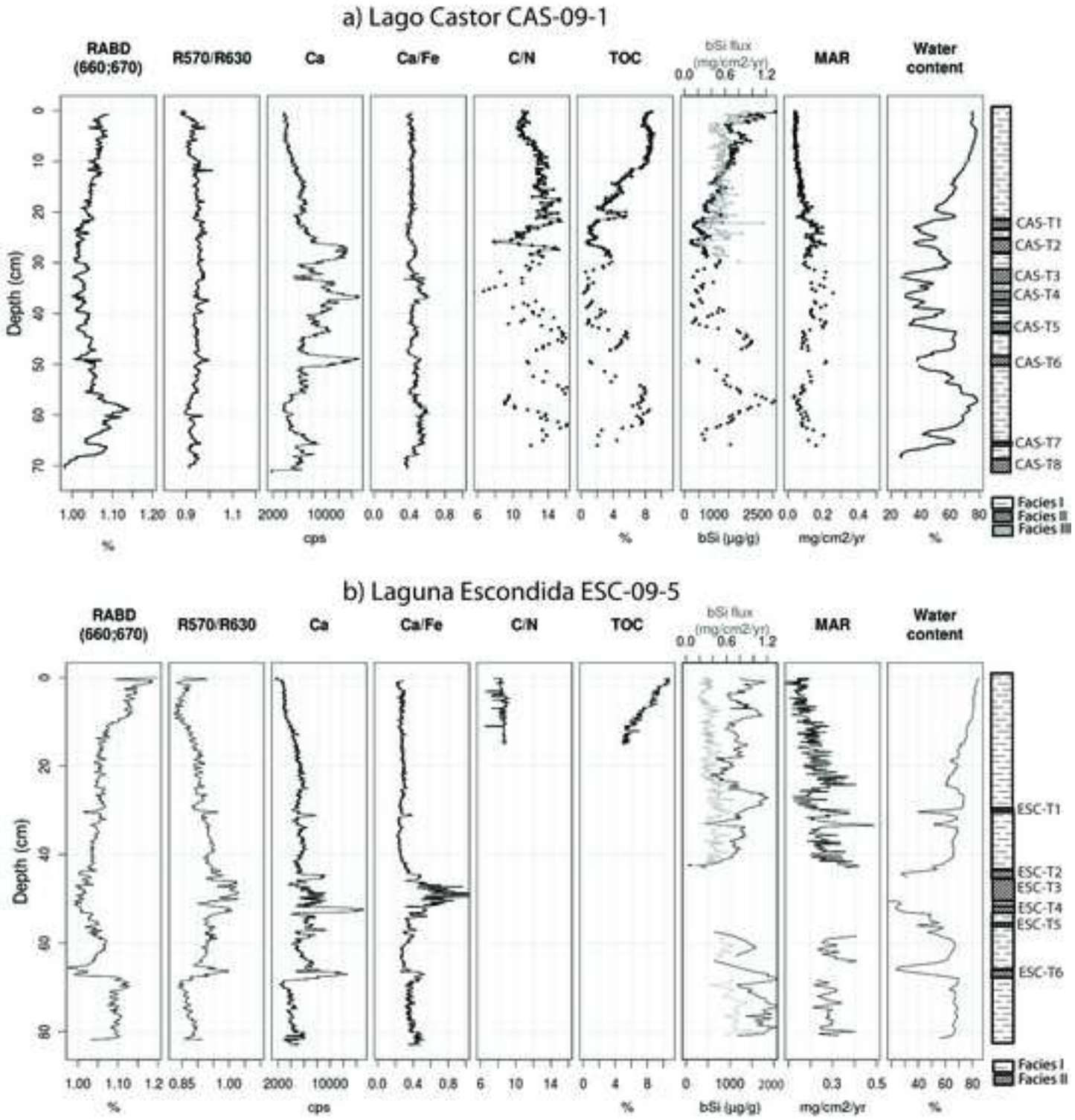

Figure4

Click here to download high resolution image

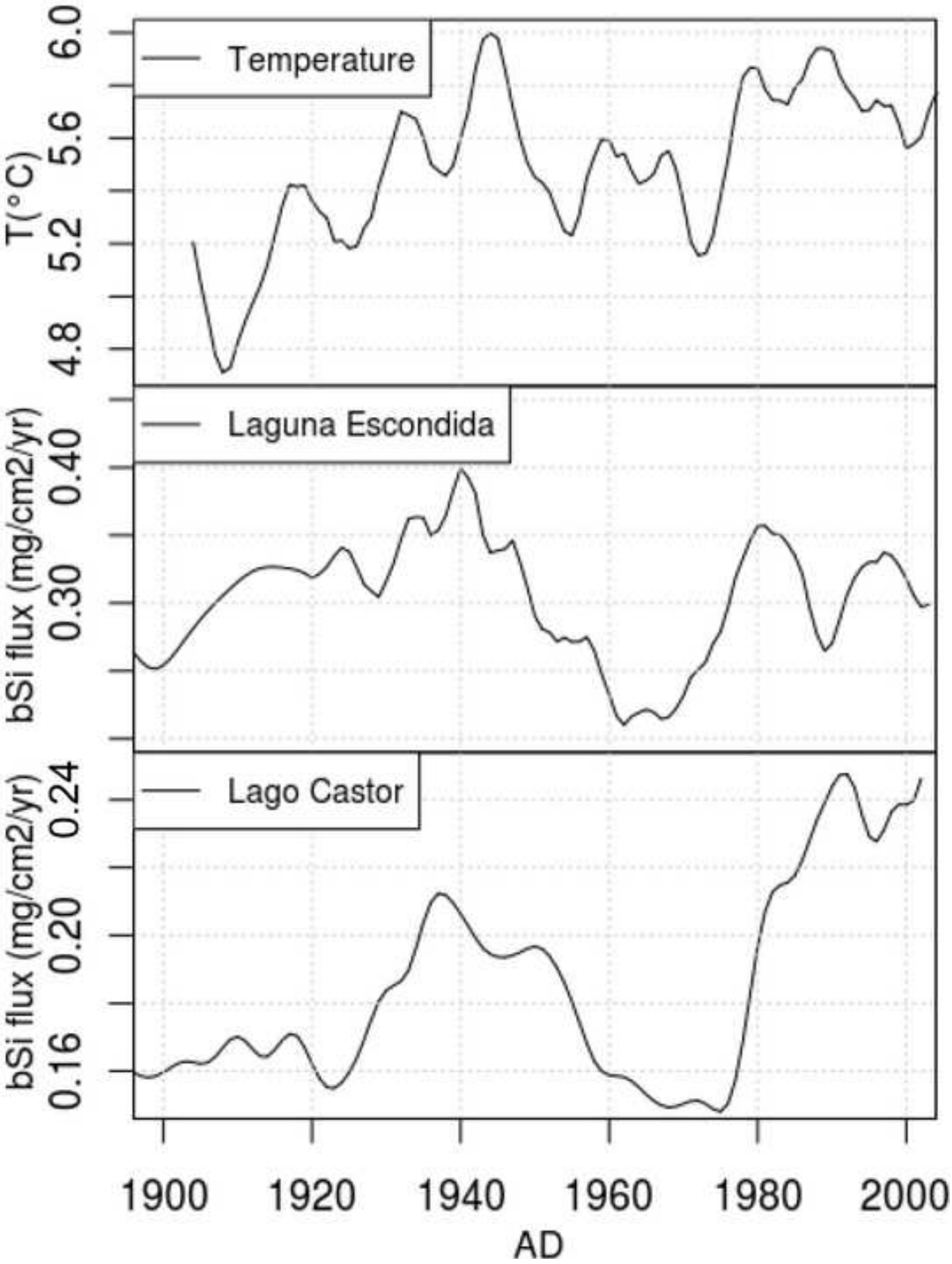

Figure5

Click here to download high resolution image

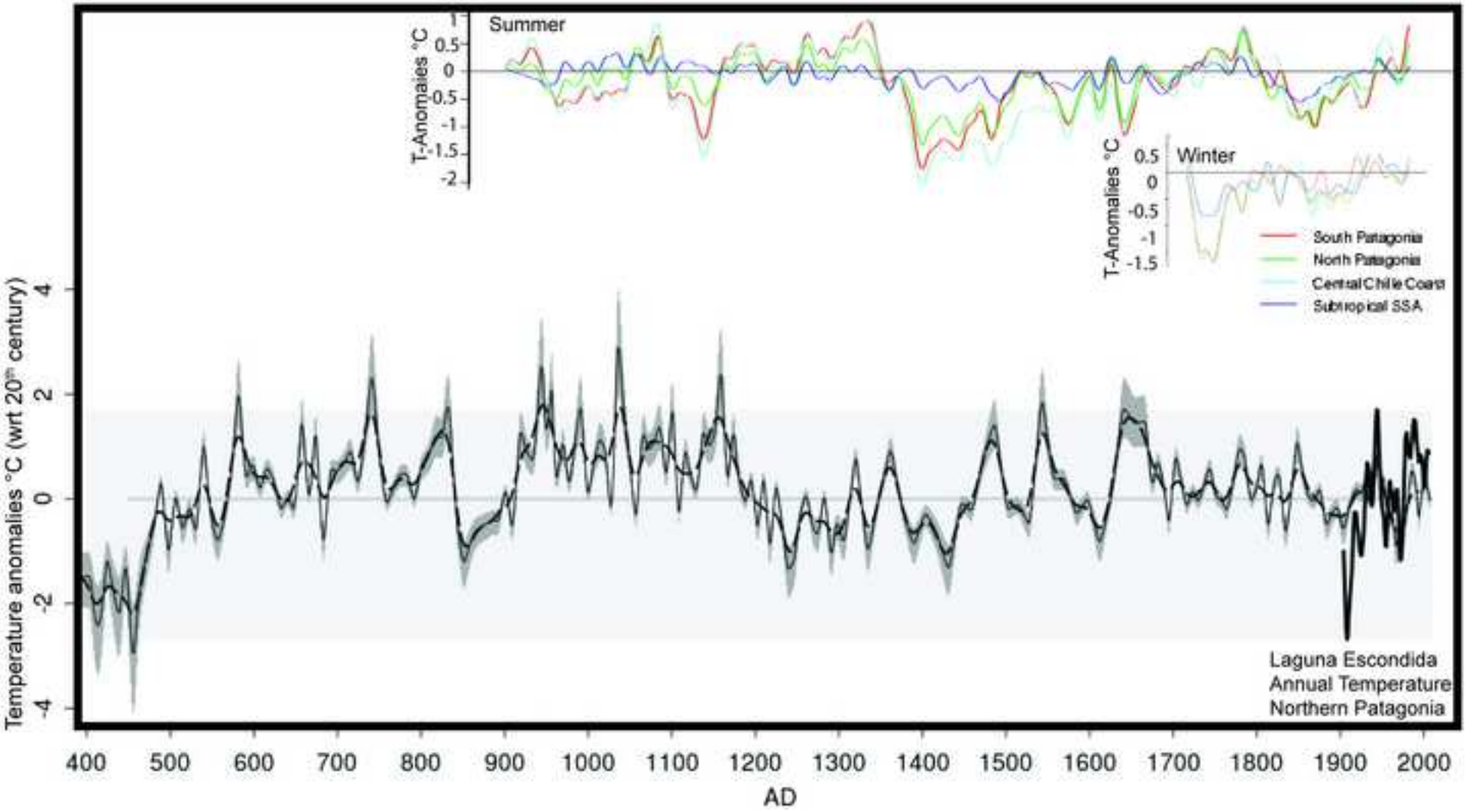

Supplementary_Figure_S1

Click here to download high resolution image

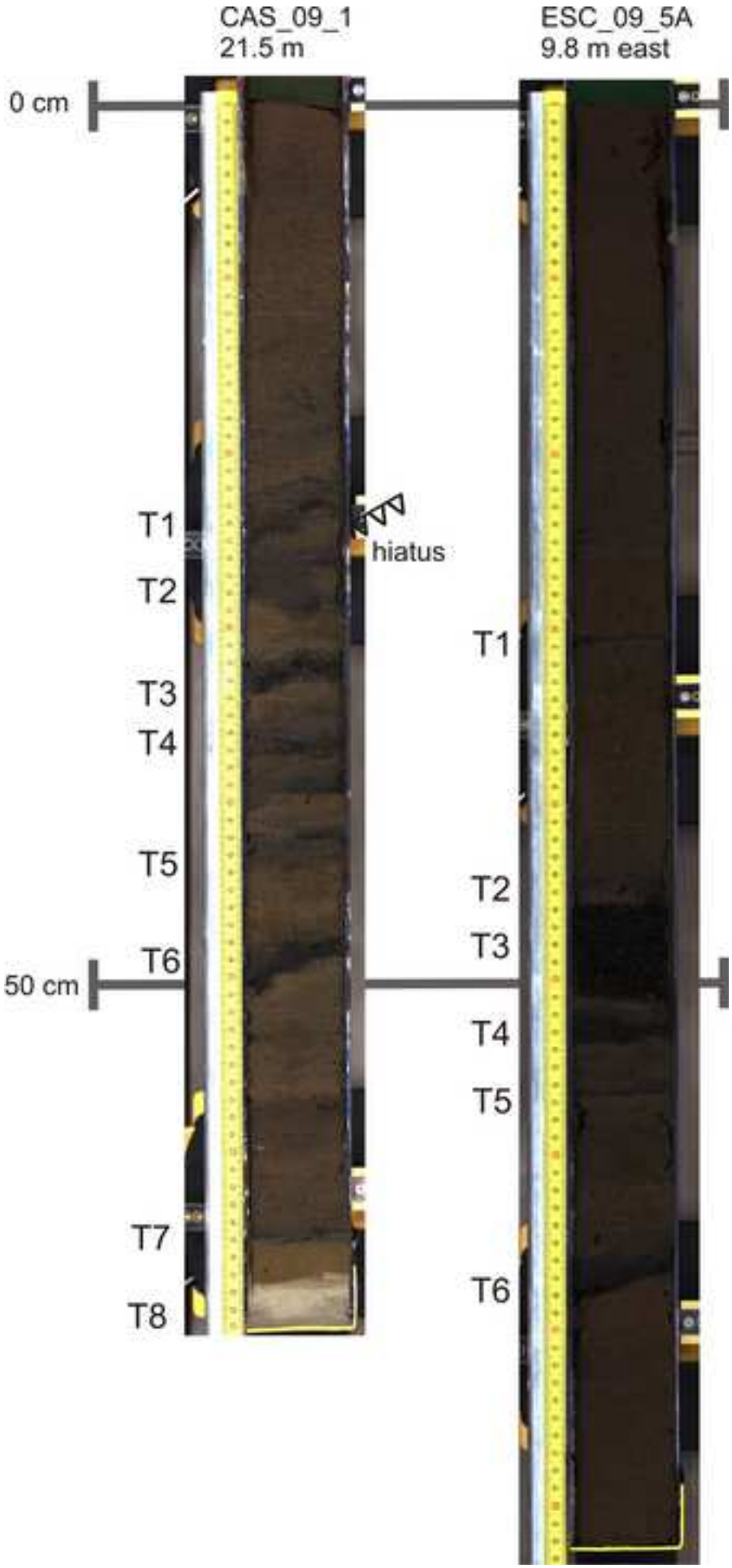

Supplementary_Figure_S2

Click here to download high resolution image

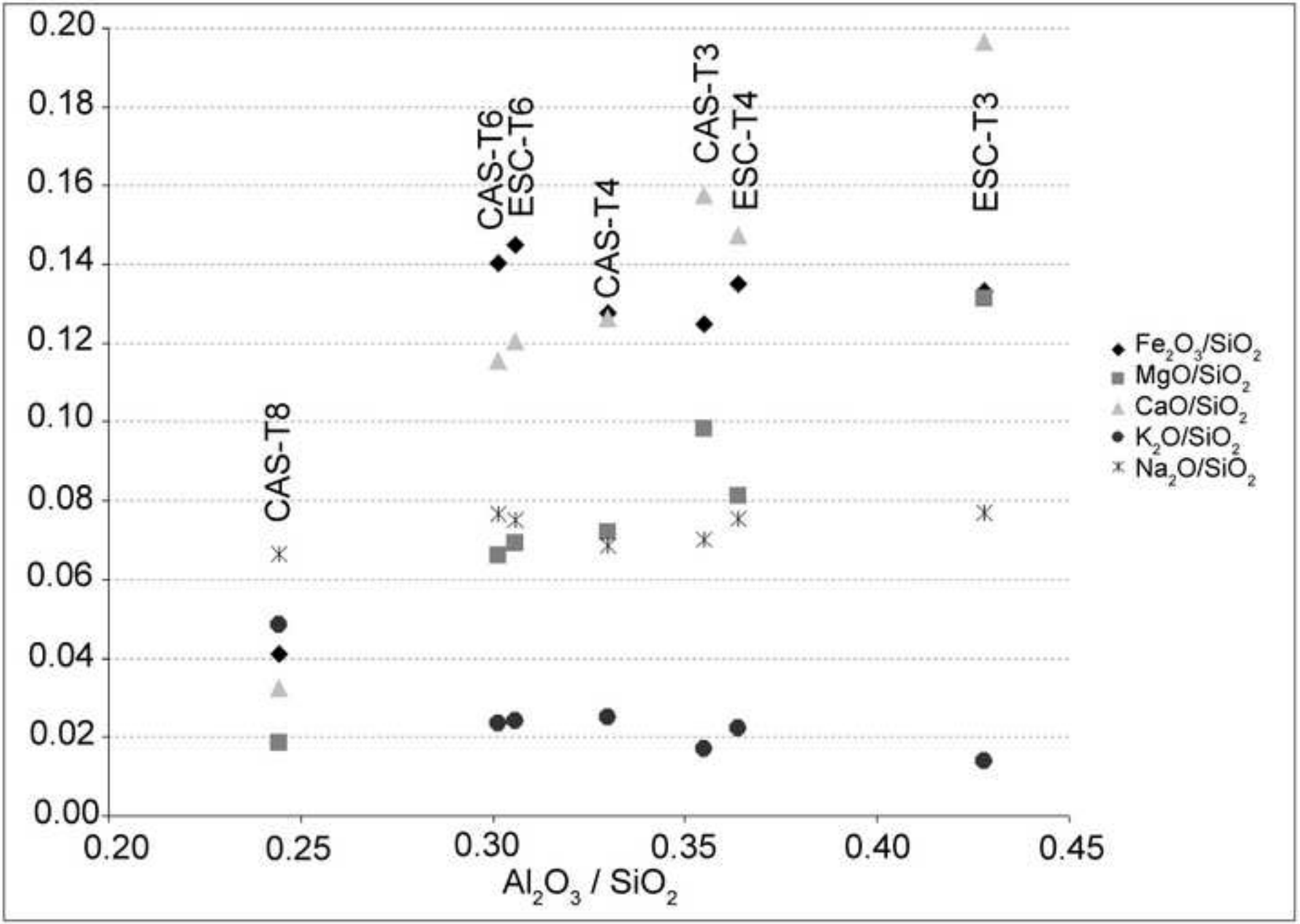

Supplementary_Figure_S3

Click here to download high resolution image

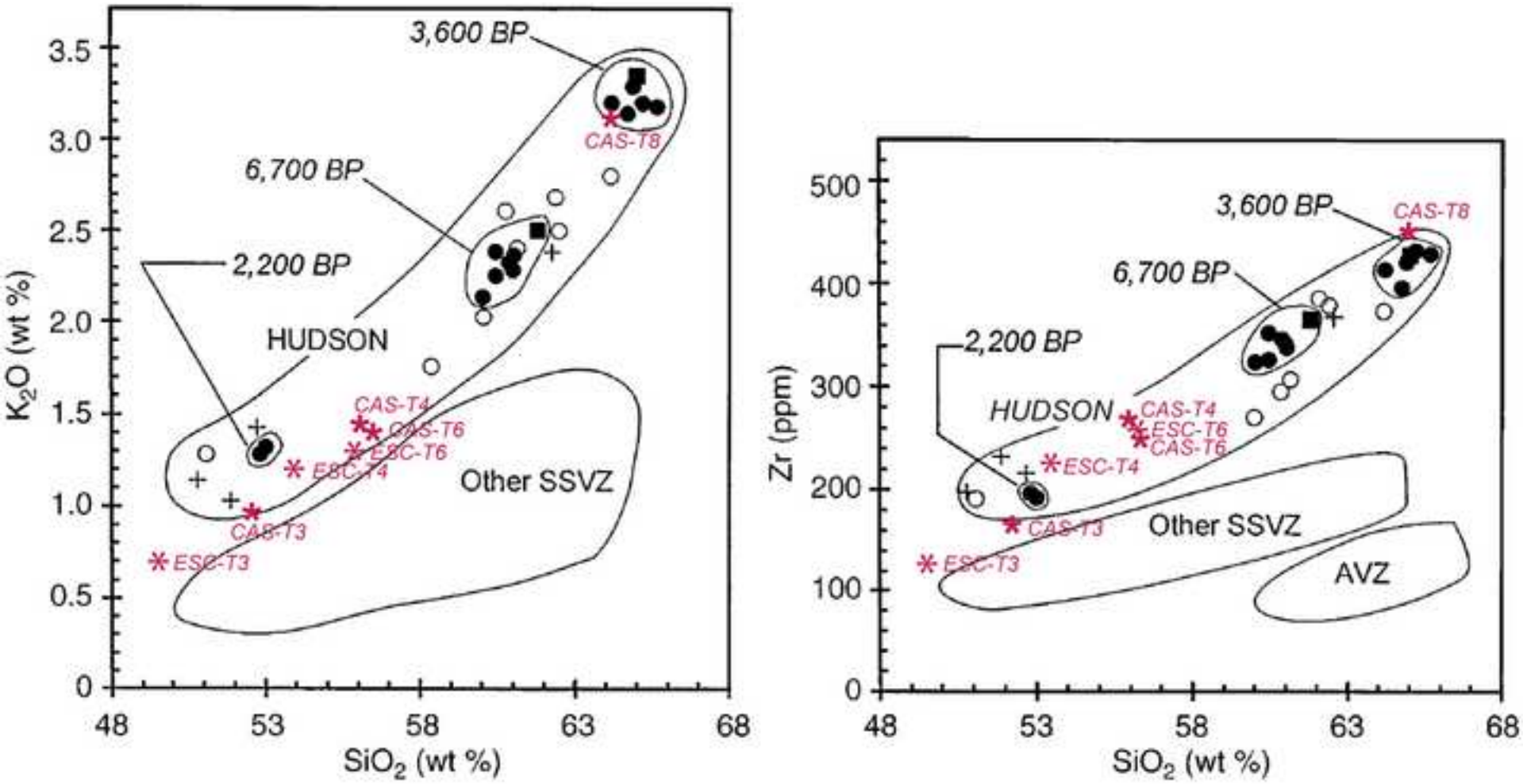

Table1

Click here to download high resolution image

14 C samples

Lab code	*Sediment Depth(cm)*	*Material*	*14C yr BP*	*Calibrated Midpoint*	*± sigma range*
Lago Castor:					
Beta - 305745	14.6-15.2	bulk	570 ± 30	AD 1410	AD 1328 - 1445
Poz-33733	17.8-18.3	bulk	795 ± 30	AD 1259	AD 1220 -1291
Poz-33734	23.1-23.6	bulk	1040 ± 30	AD 1099	AD 1166 - 1039
Beta-305746	23.8-24.2	bulk	1400 ± 30	AD 682	AD 636 - 769
Beta - 305747	25.6-26.0	bulk	1580 ± 30	AD 530	AD 430 - 608
Poz-31858	30.5-31.5	bulk	1930 ± 30	AD 162	AD 71 - 244
Beta - 305748	51.6-52.0	bulk	2500 ± 30	BC 567	BC 753 - 402
Poz-31859	60.0-61.0	bulk	3125 ± 35	BC 1333	BC 1432 - 1218
Poz-3860	60.0-61.0	leaf remain	3100 ± 35	BC 1320	BC 1415 - 1133
Laguna Escondida:					
Poz-34647	20.0-20.5	bulk	760 ± 30	AD 1297	AD 1231 - 1384
Poz-31861	29.5-30.5	bulk	1155 ± 30	AD 942	AD 881 - 1004
Poz-31862	80.5-81.5	bulk	2805 ± 35	BC 892	BC 987 - 809

Supplementary_Table_S1

Click here to download high resolution image

Name:	Depth (cm)	Thickness (cm)	Age
ESC-09-5			
ESC-T1	30.2 - 30.5	0.3	AD 950
ESC-T2	44.0 - 45.0	1.0	AD 400
ESC-T3	45.5 - 51.0	5.5	AD 160
ESC-T4	52.0 - 53.5	1.5	AD 90
ESC-T5	56.5 - 56.7	0.2	BC 50
ESC-T6	66.0 - 68.0	2.0	BC 300
CAS-09-1			
CAS-T2	28.0 - 29.0	1.0	AD 400
CAS-T3	32.0 - 34.0	2.0	AD 160
CAS-T4	36.0 - 37.5	1.5	AD 90
CAS-T5	42.5 - 43.0	0.5	BC 50
CAS-T6	48.0 - 49.0	1.0	BC 300
CAS-T7	65.0 - 65.2	0.2	BC 1700
CAS-T8	68.0 - 70.0+	>2.0	BC 1950

Supplementary_Table_S2

Click here to download high resolution image

	ESC T3	ESC T3*	ESC T4	ESC T4*	ESC T6	ESC T6*	CAS T3	CAS T3*	CAS T4	CAS T4*	CAS T6	CAS T6*	CAS T8
SiO_2	49.4	50.2	53.3	52.9	55.8	55.8	55.3	52.1	55.8	55.7	56.3	56.2	64.0
TiO_2	0.8	0.8	1.2	1.2	1.5	1.5	1.6	1.0	1.2	1.2	1.5	1.5	0.5
Al_2O_3	21.2	20.8	19.4	19.2	17.1	17.2	17.2	19.6	18.4	18.4	17.0	17.1	15.7
Fe_2O_3	6.6	6.7	7.2	7.2	8.1	7.9	8.2	6.9	7.1	7.2	7.9	8.0	2.6
MnO	0.1	0.1	0.1	0.1	0.1	0.1	0.1	0.1	0.1	0.1	0.1	0.1	0.1
MgO	6.5	6.7	4.3	4.4	3.9	3.7	3.7	5.4	4.0	3.8	3.7	3.7	1.2
CaO	9.7	10.0	7.9	7.8	6.7	6.6	6.6	8.7	7.0	7.1	6.5	6.5	2.1
K_2O	0.7	0.7	1.2	1.2	1.3	1.4	1.4	0.9	1.4	1.3	1.3	1.3	3.1
Na_2O	3.8	3.1	4.0	4.5	4.2	4.4	4.4	3.9	3.8	4.0	4.3	4.1	4.3
P_2O_5	0.4	0.4	0.5	0.5	0.7	0.6	0.7	0.5	0.5	0.6	0.7	0.7	0.1
Rb_2O	0.0	0.0	0.0	0.0	0.0	0.0	-	0.0	0.0	0.0	0.0	0.0	0.0
SrO	0.1	0.1	0.1	0.1	0.1	0.1	0.1	0.1	0.1	0.1	0.1	0.1	0.0
Y_2O_3	-	-	0.0	0.0	-	0.0	0.0	0.0	0.0	0.0	0.0	0.0	0.0
ZrO_2	0.0	0.0	0.0	0.0	0.0	0.0	0.0	0.0	0.0	0.0	0.0	0.0	0.1
Cs_2O	0.1	0.1	0.1	0.1	0.1	0.0	-	-	-	-	-	-	-
PbO	0.0	0.0	0.0	0.0	0.0	0.0	-	-	-	-	-	-	-